RSC Advances

RSC Publishing

PAPER

View Article Online
View Journal | View Issue

Cite this: *RSC Advances*, 2013, **3**, 9764

Rapid, low temperature microwave synthesis of durable, superhydrophobic carbon nanotube–polybenzoxazine nanocomposites

Chih-Feng Wang,*[a] Hsuan-Yu Chen,[a] Shiao-Wei Kuo,[b] Yi-Shao Lai[c] and Ping-Feng Yang[c]

Received 19th February 2013,
Accepted 9th April 2013

DOI: 10.1039/c3ra40827b

www.rsc.org/advances

In this study we used microwave irradiation at 2.45 GHz to synthesize superhydrophobic multi-wall carbon nanotube (MWCNT)–polybenzoxazine (PBZ) nanocomposites. The process required only approximately 45 s to ensure complete polymerization. The MWCNT–PBZ nanocomposites, which do not contain any fluorinated compounds, maintained their superhydrophobicity after pressing and displayed excellent environmental stability. From studies of the impact behavior of water droplets, we found that the microwave-treated MWCNT–PBZ nanocomposites exhibited robust superhydrophobicity under dynamic conditions, with the droplets bouncing off their surfaces completely without wetting. Furthermore, the superhydrophobic MWCNT–PBZ nanocomposites had excellent stability in terms of the contact angle with water after to organic solvent treatment .

Introduction

The performance of a solid material is often dictated by its surface properties, such as its wettability.[1] Although the chemical composition has a great influence on wettability, it has certain limitations. Chemical modification alone, with fluoropolymeric coatings or fluorinated silane layers, can lead to the water contact angles of flat surfaces reaching up to 120°. Nevertheless, superhydrophobic surfaces require water contact angles exceeding 150° and sliding angles of less than 10°.[2,3] To exhibit superhydrophobicity, hydrophobic surfaces must generally be created with micro- and nanostructured roughness. While the surface roughness increases the surface area, and thus enhances the hydrophobicity (according to the Wenzel model),[4] the air trapped within the grooves beneath the liquid leads to superhydrophobic behavior because the drop sits partially on air (as proposed by the Cassie model).[5] Over the past 20 years, there have been many reported processes for the preparation of superhydrophobic surfaces,[6–10] but the stringent experimental conditions, sophisticated techniques, and tedious fabrication procedures have heretofore limited their practical applications.

Carbon nanotubes (CNTs) have found enormous applicability in many areas of science and engineering because of their excellent electronic, mechanical, and chemical properties. Nevertheless, the effects of microwave irradiation on the thermal properties of CNTs have received only limited attention. Microwaves are a form of electromagnetic radiation with frequencies ranging approximately from 300 MHz to 300 GHz. Recently, it has been demonstrated that single-walled carbon nanotubes (SWCNTs)[11] and multi-walled carbon nanotubes (MWCNTs)[12] exhibit strong microwave absorbing characteristics that lead to intense heat, outgassing, and light emission.[11] The results of several researchers have been particularly notable. Chin *et al.*[13] reported that MWCNTs could be welded onto polymer substrates [*e.g.*, polycarbonate, poly(ethylene terephthalate)] through microwave irradiation for a few seconds; furthermore, they developed the use of MWCNTs as a solder to bond polymeric substrates together. Gu and co-workers[14] used a microwave curing method to prepare MWCNT–epoxy composites possessing a very high dielectric constant and low dielectric loss. Ng *et al.*[15] developed a new technology for forming hollow MWCNT–poly(methyl methacrylate) nanocomposite cylinders through microwave exposure. Superhydrophobic phenomena have been observed for aligned and non-aligned CNT films.[16–18] However, multi-step processes, stringent preparation specifications and the long production times required to form superhydrophobic CNT films have heretofore limited their practical applications

In a previous study, we discovered a new class of non-fluorine and non-silicon low surface free energy polymeric

[a]*Department of Materials Science and Engineering, I-Shou University, Kaohsiung, 840, Taiwan E-mail: cfwang@isu.edu.tw; Fax: 886-7-6578444; Tel: 886-7-6577711-3129*
[b]*Department of Materials and Optoelectronic Science, Center for Nanoscience and Nanotechnology, National Sun Yat-Sen University, Kaohsiung, 804, Taiwan*
[c]*Central Product Solutions, Advanced Semiconductor Engineering, Inc., Kaohsiung, 811, Taiwan*

materials: polybenzoxazines (PBZs).[19] PBZs feature surface free energies even lower than that (21 mJ m^{-2}) of pure polytetrafluoroethylene (PTFE). Although PBZs and fluoropolymers both possess low surface free energies, the former are cheaper to prepare and easier to process. Furthermore, PBZs have other attractive properties, including high glass transition temperatures, excellent resistance to chemicals, and a low degree of water absorption.[20] Nevertheless, the need for high-temperature curing and long production times restricted the broader applications of PBZ composites. Herein, we introduce a simple and rapid method for fabricating durable superhydrophobic CNT–PBZ nanocomposites through microwave curing. The as-prepared nanocomposites possessed high water contact angles (*ca.* 165°) and very low sliding angles (4°), allowing the rolling of water droplets, thus suggesting a self-cleaning ability. Furthermore, the use of commercially available raw materials and simple fabrication and operation processes suggests the possibility to apply such surfaces to academic research and industrial applications.

Experimental

2,2-Bis(3-phenyl-3,4-dihydro-2*H*-1,3-benzoxazinyl)propane (BA-a benzoxazine, BZ) was supplied by Shikoku Chemicals Corp. MWCNTs (average diameter: 20–40 nm; length: 5–15 μm) were purchased from Conyuan Biochemical Technology. These materials were used as received. Water that had been purified through reverse osmosis was further purified using a Millipore Milli-Q system.

MWCNT–PBZ nanocomposites were prepared on glass slides using a deposition method. First, a BZ solution was prepared by dissolving BZ (10.0 mg) in tetrahydrofuran (THF, 10 mL) and then filtering through a 0.2 μm syringe filter. MWCNTs (10.0 mg) were added to the BZ solution, which was subjected to ultrasonication for 2 h. The MWCNT–BZ suspension was poured onto a glass slide in an aluminum container and then the sample was left to dry at room temperature for 5 h to form a MWCNT–BZ nanocomposite, which was cured through heating in an oven (240 °C, 1 h) or microwave irradiation (1100 W, 2.45 GHz, 45 s). The MWCNT–PBZ nanocomposites prepared through thermal and microwave curing are denoted herein as t-MWCNT–PBZ and m-MWCNT–PBZ, respectively.

The microstructures of the MWCNT–PBZ nanocomposites were characterized using a HITACHI-S-4700 scanning electron microscope (acceleration voltage: 15 kV); each specimen was coated with a thin layer of Pt/Pd prior to observation. Contact angles and sliding angles were measured using a FDSA MagicDroplet-100 contact angle goniometer. The static contact angles and sliding angles were measured from a single drop (*ca.* 5 μL). Each reported contact angle represents the average of six measurements. The curing behaviors of the BZ and the MWCNT–BZ nanocomposite were determined through differential scanning calorimetry (DSC) using a TA Q20 instrument (scan rate: 20 °C min^{-1}; temperature range: 25–280 °C). Thermogravimetric analysis (TGA) was performed under N_2 using a TA Instruments Q50 apparatus (heating rate: 20 °C min^{-1}; temperature range: from room temperature to 800 °C. N_2 flow rate: 60 mL min^{-1}). The film's durability to solvents was evaluated by immersing it in an organic solvent for 24 h and then drying at 60 °C. The pencil hardness of the superhydrophobic films was determined using the method described in ASTMD 3363, a standard test method for film hardness. The tape test was performed according to ASTM D 3359-02, a standard test for measuring adhesion.

Results and discussion

After spin-coating BZ onto a glass slide and then curing at 240 °C for 1 h, we obtained a smooth surface. The water contact angle of this smooth PBZ surface was approximately 110°; although hydrophobic, this value is too low for this material to be classified as superhydrophobic.

Combining BZ with MWCNTs provided superhydrophobic coatings on the glass slides. We poured MWCNT–BZ suspensions onto glass slides in an aluminum container and then left the sample to dry at room temperature. Although the as-prepared MWCNT–BZ nanocomposites possessed high water contact angles (159 ± 2°) and low sliding angles (7°), the poor thermal and mechanical properties of these superhydrophobic coatings would seriously limit their industrial applications. Accordingly, we cured these MWCNT–BZ nanocomposites in an oven (240 °C, 1 h) to obtain t-MWCNT–PBZ nanocomposites. The chemical resistance, thermal stability, and mechanical durability of these t-MWCNT–PBZ nanocomposites were improved compared with those of the MWCNT–BZ nanocomposites. Although bulk cross-linking had only a negligible effect on their water repellency, the t-MWCNT–PBZ nanocomposites retained the superhydrophobicity of the MWCNT–BZ nanocomposites, with high contact angles (164 ± 1°) and low sliding angles (4°). Nevertheless, the need for curing at high-temperature (240 °C) for a long time (1 h) restricts the broader applications of these t-MWCNT–PBZ nanocomposites. In a previous study,[21] we discovered that BZ can be cured at a relatively low temperature (120 °C) with the aid of 2,2′-azoisobutyronitrile (AIBN), resulting in a low surface energy, but this process still requires a long production time (8 h). Knowing that CNTs strongly absorb microwaves at specific frequencies with intense heat release and rapid temperature increases, we found that our MWCNT–BZ nanocomposites could be cured rapidly – within 45 s at room temperature – to form m-MWCNT–PBZ nanocomposites under microwave irradiation. To the best of our knowledge, this method is the fastest ever reported for preparation of PBZ nanocomposites.

We used DSC to monitor the curing behavior of the BZ monomer in the presence of MWCNTs. Fig. 1 presents the DSC curves of the pure BZ monomer; and the MWCNT–BZ, t-MWCNT–PBZ, and m-MWCNT–PBZ nanocomposites. Relative to the pure BZ monomer, the addition of MWCNTs caused the exotherm of the mixture to be shifted to the lower

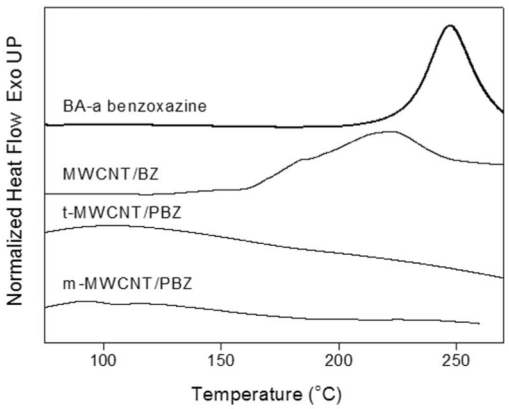

Fig. 1 DSC traces of BZ and the MWCNT–BZ, t-MWCNT–PBZ, and m-MWCNT–PBZ nanocomposites.

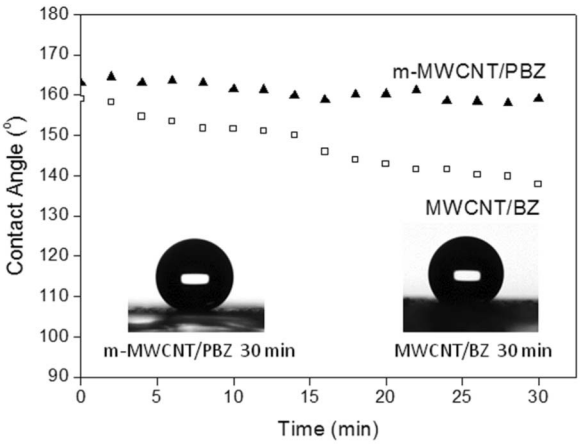

Fig. 3 Time dependence of the water contact angle of the MWCNT–BZ and m-MWCNT–PBZ nanocomposites.

temperature range, which was not only because of the high thermal conductivity of the nanotubes, but also because of their larger specific surface area.[22,23] For both the t-MWCNT–PBZ and m-MWCNT–PBZ nanocomposites, the exotherm disappeared, indicating that the curing reactions were complete after thermal curing or microwave irradiation, respectively. The m-MWCNT–PBZ nanocomposites also exhibited superhydrophobicity with high contact angles (164 $\pm$ 1°, Fig. 2a) and water droplets readily moving when their surfaces were tilted slightly (sliding angle: 3°). Although both t-MWCNT–PBZ and m-MWCNT–PBZ nanocomposites exhibited superhydrophobicity, the preparation of latter was faster; therefore, only the m-MWCNT–PBZ nanocomposites are discussed hereafter.

Fig. 2b–d present top-view scanning electron microscopy (SEM) images of m-MWCNT–PBZ nanocomposites at different magnifications. These rough substrates possessed both micro- and nano-scale binary structures: each micro-island (7–50 μm) on the m-MWCNT–PBZ surface (Fig. 2b) was covered with branch-like nanostructures (Fig. 2c). Nanostructures were also present on the lower surface of the superhydrophobic film (Fig. 2d). Such binary structures are similar to that of the self-cleaning lotus leaf; they dramatically increased the surface roughness, leading to the formation of composite interfaces[24] in which air is trapped within the grooves beneath the liquid. This phenomenon significantly minimizes the contact area between the m-MWCNT-PBZ surface and the liquid. On these m-MWCNT–PBZ nanocomposite surfaces, water droplets possessed near-spherical shapes and they rolled off with ease.

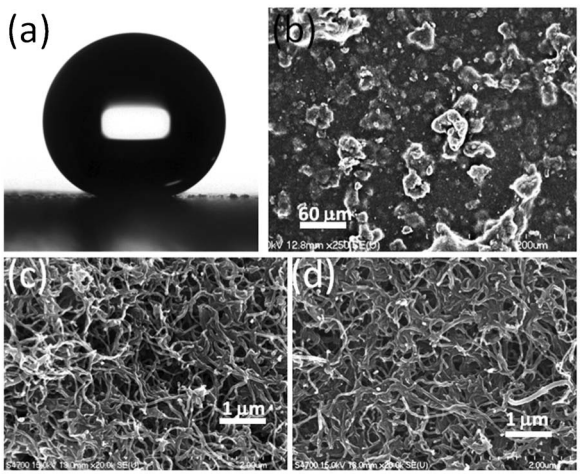

Fig. 2 (a) Profile of a water drop on the m-MWCNT–PBZ superhydrophobic surface. (b) Large-area SEM image of the m-MWCNT–PBZ superhydrophobic surface. (c) Enlarged view of a micro-island in (b). (d) SEM image of the lower surface of the superhydrophobic film.

Fig. 3 displays the time dependence of the water contact angles for the MWCNT–BZ and m-MWCNT–PBZ nanocomposites. The water contact angle of the MWCNT–BZ nanocomposite decreased linearly over time, from an initial value of 160° to 137° within 30 min. In contrast, the water droplets on the m-MWCNT–PBZ surface kept near-spherical shapes throughout the same period of time (and they could still be moved easily after 30 min), suggesting stable superhydrophobicity. Surface superhydrophobicity is usually evaluated using a combination of static contact angles and sliding angles. Notably, however, superhydrophobic surfaces, including lotus leaves and artificial materials, often lose their functionality[25] when droplets are squeezed or impacted onto them. To further explore the robustness of our MWCNT–BZ and m-MWCNT–PBZ nanocomposites, we performed compression experiments[25,26] in which we squeezed 5 μL sized water droplets between two identical substrates and then slowly released the pressure, until the initial distance between the plates was restored. For the m-MWCNT–PBZ nanocomposite system, the sequence of photographs in Fig. 4a reveals that the droplet flattened and the contact angle gradually decreased (from 159 $\pm$ 2° to 138 $\pm$ 3°) upon increasing the drop's internal pressure from 85 to 340 Pa. Remarkably, the droplet recovered its original shape when we released the pressure, revealing robust superhydrophobicity over an extended range of compression. In contrast, Fig. 4b reveals that the water contact angle did not

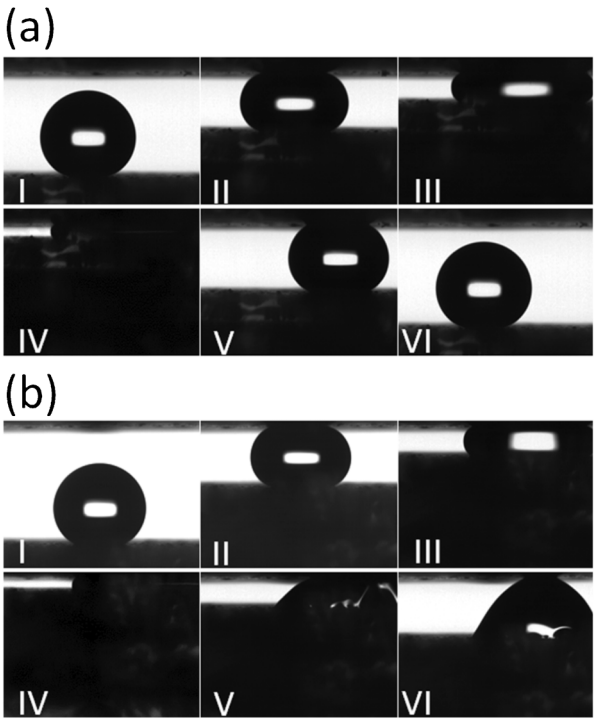

Fig. 4 Behavior of a 4 μL sized water droplet positioned between two identical substrates covered with (a) m-MWCNT–PBZ and (b) MWCNT–BZ nanocomposites.

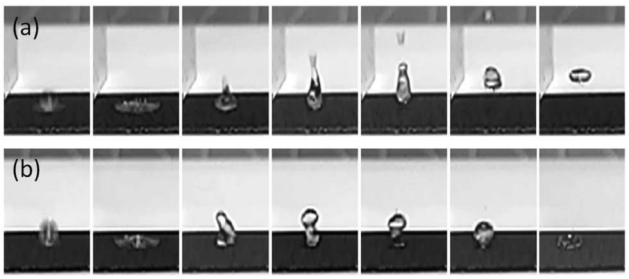

Fig. 5 Time sequence images of a water droplet falling freely onto the surfaces of (a) m-MWCNT–PBZ and (b) MWCNT–BZ nanocomposites (velocity: 0.99 m s^{-1}; height of release: 50 mm).

recover its initial value in the MWCNT–BZ nanocomposite system: the compressed droplet partially wetted the MWCNT–BZ surface, leading to a decrease in the contact angle (from 158° to 62°) and to strong adhesion, highlighting the fragile superhydrophobicity of the MWCNT–BZ nanocomposites. We were also interested in the dynamic behavior of water on the MWCNT–BZ and m-MWCNT–PBZ nanocomposites. Droplet impact experiments can be used not only to evaluate the robustness of the air gaps on fabricated superhydrophobic surfaces, but also to further our understanding of the mechanics of impact-induced droplet transitions on superhydrophobic surfaces.[27–29] On a macroscopic level, we compared the behavior of water droplets having a diameter of 3.6 mm and a velocity of 0.99 m s^{-1} impinging on the m-MWCNT–PBZ and MWCNT–BZ nanocomposites. We captured these processes using a high-speed camera; Fig. 5 presents a selected sequence of the images recorded over time. Fig. 5a reveals the behavior of a droplet falling onto the surface of the m-MWCNT–PBZ nanocomposite. The droplet initially deformed and flattened into a pancake shape, but then retracted and finally rebounded off the surface without penetrating the nanostructure. After several more bounces, the droplet eventually bounced off the surface without ever coming to rest. Nevertheless, not all of the superhydrophobic surfaces achieved the same behavior of bouncing off the surface; when the surface lacked a sufficiently low surface free energy or possessed sufficient geometrical spacing between the nanoscale structures, the wetting state of the droplet led to partial pinning at the contact area. In contrast, on the MWCNT–BZ surface (Fig. 5b), the droplet spreads but did not rebound or lift-off from the surface; eventually the water droplet came to rest by wetting the surface. These observations reveal that rapid microwave curing lowered the surface free energy of PBZ and provided robust superhydrophobic m-MWCNT–PBZ nanocomposites.

We also evaluated the effect of treatment with organic solvents on the wettability, measured relative to the contact angle measurement of pure water. Fig. 6a reveals the water contact angles of m-MWCNT–PBZ nanocomposite after treat-

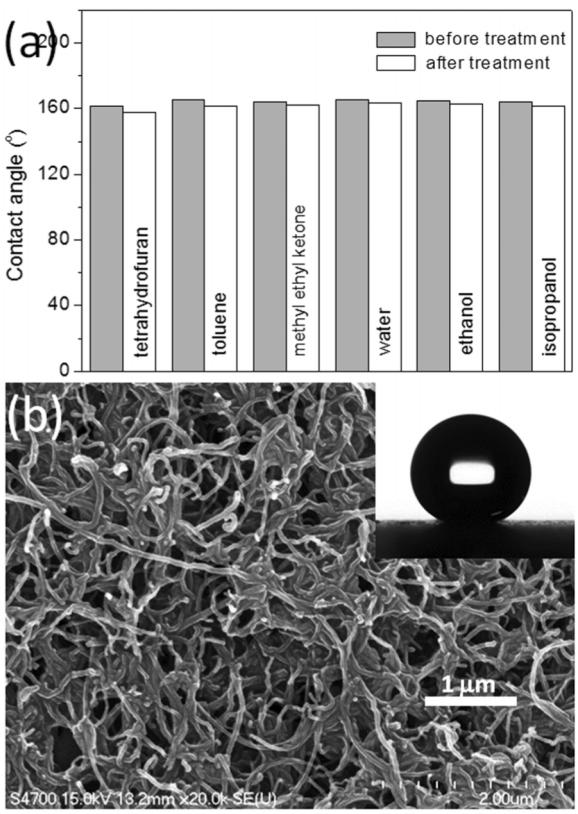

Fig. 6 (a) Durability of the superhydrophobic films after treatment with organic solvents. (b) SEM images of the m-MWCNT–PBZ nanocomposite after performing the tape test. Inset: Photograph of a water droplet on this sample.

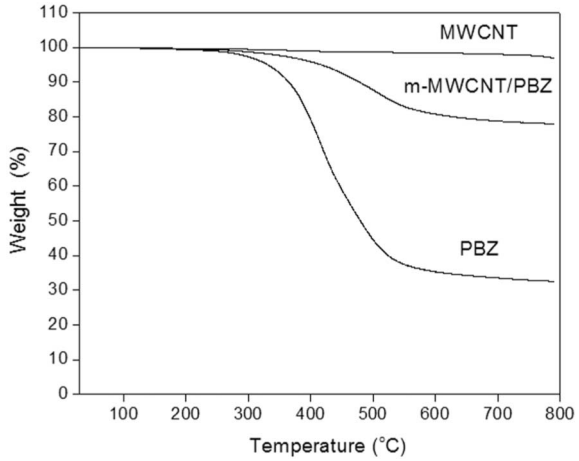

Fig. 7 TGA traces of crude MWCNTs, the PBZ and the m-MWCNT–PBZ nanocomposite under N_2.

ment with various organic solvents. The contact angles of the composites remained nearly unchanged after treatment. The adhesion of the m-MWCNT–PBZ nanocomposites to the substrates was investigated by using a Scotch tape test, based on the ASTM D3359-02 standard. In this test, we pressed the tape against the coating and then peeled it off. Fig. 6b presents SEM images of the m-MWCNT–PBZ nanocomposite after performing the tape test. Compared with the image of the original film (Fig. 2c), the surface morphology changed to only a minor degree. Therefore, the m-MWCNT–PBZ nanocomposites adhered relatively strongly to the substrate; in addition, they retained their superhydrophobicity (contact angle: 159 $\pm$ 3°, sliding angle: 5°) after performing the adhesion tests. A pencil scratch test revealed that the hardness of the m-MWCNT–PBZ nanocomposite was between H and 2H; for comparison, the MWCNT–BZ nanocomposite's hardness was between 6B and 5B. Next we used TGA to investigate the thermal properties of the m-MWCNT–PBZ nanocomposites. Fig. 7 reveals that the decomposition of the m-MWCNT–PBZ nanocomposites was delayed relative to that of the pristine PBZ. The temperatures required for a loss of 5 wt% of the m-MWCNT–PBZ nanocomposites and PBZ were 417 °C and 331 °C, respectively, indicating that the thermal stability of PBZ was improved after hybridization with MWCNTs at the nanometer level. The char yields of the m-MWCNT–PBZ nanocomposites were as high as 78 wt% at 790 °C. From measurements of their superhydrophobicity at different time intervals, we found that these films were stable after at least 12 months under ambient atmospheric conditions without any major changes in their water contact angles.

Conclusions

We have employed MWCNTs as an internal heat source for the synthesis of MWCNT–PBZ nanocomposites under microwave irradiation. The released heat allowed the BZ monomers to be cured completely within 45 s under ambient atmospheric conditions to produce MWCNT–PBZ nanocomposites exhibiting durable superhydrophobicity. These nanocomposites were sufficiently robust so that pressing processes, tape tests and treatment with organic solvents did not affect their superhydrophobicity. We also investigated the stability of the fabricated superhydrophobic surfaces under dynamic conditions through measurements of water droplet impact dynamics. Droplets on the m-MWCNT–PBZ nanocomposites rebounded off the surfaces cleanly. We believe that these readily prepared materials will be useful in academic research and industrial applications.

Acknowledgements

This study was supported financially by the National Science Council, Taiwan, Republic of China, under contract NSC 101-2221-E-214-012.

References

1 H. Gau, S. Herminghaus, P. Lenz and R. Lipowsky, *Science*, 1999, **283**, 46–49.
2 X. Yao, Y. Song and L. Jiang, *Adv. Mater.*, 2011, **23**, 719–734.
3 O. Sato, S. Kubo and Z. Z. Gu, *Acc. Chem. Res.*, 2009, **42**, 1–10.
4 R. N. Wenzel, *Ind. Eng. Chem.*, 1936, **28**, 988–994.
5 A. B. D. Cassie and S. Baxter, *Trans. Faraday Soc.*, 1944, **40**, 546–551.
6 S. Nishimotoab and B. Bhushan, *RSC Adv.*, 2013, **3**, 671–690.
7 L. Shen, H. Ding, Q. Cao, W. Jia, W. Wang and Q. Guo, *Carbon*, 2012, **50**, 4284–4290.
8 J. Sun and B. Bhushan, *RSC Adv.*, 2012, **2**, 12606–12623.
9 A. Raza, Y. Si, X. Wang, T. Ren, B. Ding, J. Yu and S. S. Al-Deyab, *RSC Adv.*, 2012, **2**, 12804–12811.
10 K. Liu and L. Jiang, *Nano Today*, 2011, **6**, 155–175.
11 T. J. Imholt, C. A. Dyke, B. Hasslacher, J. M. Perez, D. W. Price, J. A. Roberts, J. B. Scott, A. Wadhawan, Z. Ye and J. M. Tour, *Chem. Mater.*, 2003, **15**, 3969–3970.
12 C. Y. Wang, T. H. Chen, S. C. Chang, T. S. Chin and S. Y. Cheng, *Appl. Phys. Lett.*, 2007, **90**, 103111–3.
13 C. Wang, T. H. Chen, S. C. Chang, S. Cheng and T. S. Chin, *Adv. Funct. Mater.*, 2007, **17**, 1979–1983.
14 J. Chang, G. Liang, A. Gu, S. Cai and L. Yuan, *Carbon*, 2012, **50**, 689–698.
15 H. Wang, J. Feng, X. Hu and K. M. Ng, *Nanotechnology*, 2009, **20**, 095601.
16 H. Liu, J. Zhai and L. Jiang, *Soft Matter*, 2006, **2**, 811–821.
17 K. S. Liao, A. Wan, J. D. Batteas and D. E. Bergbreiter, *Langmuir*, 2008, **24**, 4245–4253.
18 S. C. Cho, Y. C. Hong and H. S. Uhm, *J. Mater. Chem.*, 2007, **17**, 232–237.
19 C. F. Wang, Y. C. Su, S. W. Kuo, C. F. Huang, Y. C. Sheen and F. C. Chang, *Angew. Chem., Int. Ed.*, 2006, **45**, 2248–2251.
20 H. Ishida, in *Handbook of Benzoxazine Resins*, ed. H. Ishida and T. Agag, Elsevier, 2011, pp. 3–69.

21 C. S. Liao, J. S. Wu, C. F. Wang and F. C. Chang, *Macromol. Rapid Commun.*, 2008, **29**, 52–56.
22 Q. Chen, R. Xu and D. Yu, *Polymer*, 2006, **47**, 7711–7719.
23 Y. Liu, B. Wang and X. Jing, *Polym. Compos.*, 2011, **32**, 1352–1361.
24 C. F. Wang, W. Y. Chen, H. Z. Cheng and S. L. Fu, *J. Phys. Chem. C*, 2010, **114**, 15607–15611.
25 X. Yao, Q. Chen, L. Xu, Q. Li, Y. Song, X. Gao, D. Quéré and L. Jiang, *Adv. Funct. Mater.*, 2010, **20**, 656–662.
26 J. Shieh, F. J. Hou, Y. C. Chen, H. M. Chen, S. P. Yang, C. C. Cheng and H. L. Chen, *Adv. Mater.*, 2010, **22**, 597–601.
27 K. K. S. Lau, J. Bico, K. B. K. Teo, M. Chhowalla, G. A. J. Amaratunga, W. I. Milne, G. H. McKinley and K. K. Gleason, *Nano Lett.*, 2003, **3**, 1701–1705.
28 L. H. Li and Y. Chen, *Langmuir*, 2010, **26**, 5135–5140.
29 P. Tsai, S. Pacheco, C. Pirat, L. Lefferts and D. Lohse, *Langmuir*, 2009, **25**, 12293–12298.